

Spin transport in epitaxial Fe_3O_4/GaAs lateral structured devices

Zhaocong Huang(黄兆聪), Wenqing Liu(刘文卿), Jian Liang(梁健), Qingjie Guo(郭庆杰), Ya Zhai(翟亚), and Yongbing Xu(徐永兵)

Citation: Chin. Phys. B, 2022, 31 (**6**): 068505. DOI: 10.1088/1674-1056/ac4903
Journal homepage: http://cpb.iphy.ac.cn; http://iopscience.iop.org/cpb

What follows is a list of articles you may be interested in

Magnetoresistance effect in vertical NiFe/graphene/NiFe junctions

Pei-Sen Li(李裴森), Jun-Ping Peng(彭俊平), Yue-Guo Hu(胡悦国), Yan-Rui Guo(郭颜瑞), Wei-Cheng Qiu(邱伟成), Rui-Nan Wu(吴瑞楠), Meng-Chun Pan(潘孟春), Jia-Fei Hu(胡佳飞), Di-Xiang Chen(陈棣湘), and Qi Zhang(张琦)
Chin. Phys. B, 2022, 31 (**3**): 038502. DOI: 10.1088/1674-1056/ac192e

Visualization of tunnel magnetoresistance effect in single manganite nanowires

Yang Yu(郁扬), Wenjie Hu(胡雯婕), Qiang Li(李强), Qian Shi(时倩), Yinyan Zhu(朱银燕), Hanxuan Lin(林汉轩), Tian Miao(苗田), Yu Bai(白羽), Yanmei Wang(王艳梅), Wenting Yang(杨文婷), Wenbin Wang(王文彬), Hangwen Guo(郭杭闻), Lifeng Yin(殷立峰), Jian Shen(沈健)
Chin. Phys. B, 2020, 29 (**1**): 018501. DOI: 10.1088/1674-1056/ab5932

Homogeneous and inhomogeneous magnetic oxide semiconductors

Xiao-Li Li(李小丽), Xiao-Hong Xu(许小红)
Chin. Phys. B, 2019, 28 (**9**): 098506. DOI: 10.1088/1674-1056/ab38ac

Effects of edge hydrogenation and Si doping on spin-dependent electronic transport properties of armchair boron-phosphorous nanoribbons

Hong Zhao(赵虹), Dan-Dan Peng(彭丹丹), Jun He(何军), Xin-Mei Li(李新梅), Meng-Qiu Long(龙孟秋)
Chin. Phys. B, 2018, 27 (**10**): 108504. DOI: 10.1088/1674-1056/27/10/108504

Spin-dependent transport characteristics of nanostructures based on armchair arsenene nanoribbons

Kai-Wei Yang(杨开巍), Ming-Jun Li(李明君), Xiao-Jiao Zhang(张小姣), Xin-Mei Li(李新梅), Yong-Li Gao(高永立), Meng-Qiu Long(龙孟秋)
Chin. Phys. B, 2017, 26 (**9**): 098509. DOI: 10.1088/1674-1056/26/9/098509

Spin transport in epitaxial Fe_3O_4/GaAs lateral structured devices

Zhaocong Huang(黄兆聪)[1,2], Wenqing Liu(刘文卿)[3,4], Jian Liang(梁健)[1], Qingjie Guo(郭庆杰)[1], Ya Zhai(翟亚)[1,†], and Yongbing Xu(徐永兵)[2,3,‡]

[1] *School of Physics, Southeast University, Nanjing* 211189, *China*
[2] *Spintronics and Nanodevice Laboratory, Department of Electronics, University of York, York YO*10 5*DD, United Kingdom*
[3] *York-Nanjing Joint Center in Spintronics, School of Electronic Science and Engineering, Nanjing University, Nanjing* 210023, *China*
[4] *Department of Electronic Engineering, Royal Holloway University of London, Egham, Surrey TW*20 0*EX, United Kingdom*

(Received 8 November 2021; revised manuscript received 4 January 2022; accepted manuscript online 5 January 2022)

Research in the spintronics community has been intensively stimulated by the proposal of the spin field-effect transistor (SFET), which has the potential for combining the data storage and process in a single device. Here we report the spin dependent transport on a Fe_3O_4/GaAs based lateral structured device. Parallel and antiparallel states of two Fe_3O_4 electrodes are achieved. A clear MR loop shows the perfect butterfly shape at room temperature, of which the intensity decreases with the reducing current, showing the strong bias dependence. Understanding the spin-dependent transport properties in this architecture has strong implication in further development of the spintronic devices for room-temperature SFETs.

Keywords: spin field-effect transistor, spin injection and detection, half metal, magnetoresistance

PACS: 85.75.–d, 85.75.Hh, 73.43.Qt, 75.30.Gw **DOI:** 10.1088/1674-1056/ac4903

1. Introduction

The spin transport and the spin manipulation of carrier spins represent two key elements of semiconductor (SC) spintronics logic devices including several viable types of spin transistors, particularly spin field-effect transistors (FETs).[1–3] Research on spin injection and detection and spin coherence in semiconductors continues to draw extensive interest from both the scientific and the technical communities.[4–6] The electron spin relaxation time in SCs has been revealed to be several orders of magnitude longer than the electron momentum and energy relaxation times.[7] Further experimental evidence has been proven that electrons can be transported a distance of as large as 100 μm without loss of their spin coherence using an electric field for the case of GaAs.[8] These observations suggest that spin information could be transmitted efficiently in specific SC channels. Although all electrical spin field effect transistors have been demonstrated, they operate at low temperatures and require multi-terminals or non-local geometry.[9–14] It has been predicted that the magnetoresistance (MR) effect due to diffusive electron transport may exist in a two-terminal spin-valve structure with a non-magnetic SC layer.[15,16] However, room temperature spin injection and transmission in FM/SC/FM system (FM: ferromagnet) is still challenging.

Ferromagnetic source with high spin polarization near the Fermi level has inherent advantages in spin injection. Half metallic Fe_3O_4 film in this regard is an ideal candidate due to its high Curie temperature of 858 K and large spin polarization near 100% at the Fermi level at room temperature, even though a reduction of spin polarization of Fe_3O_4 may appear due to non-stoichiometry or surface effect.[17–20] Unlike ferromagnetic metals and alloys that have a significant 'conductivity mismatch'[21–24] with the SCs,[25] Fe_3O_4 has relatively high electrical conductivity and potentially forms non-ohmic contact with SCs like GaAs.[26,27] Moreover, spin–orbit coupling (SOC) also play an important role in spin FET devices.[1,3,28] In this respect, the enhanced SOC effect near Fe_3O_4/GaAs interface[29] and two-dimensional (2D) SC as the spin transport media due to effects from 2D confinement are preference for the spin FET device. In this article, we report the fabrication and characterizations of a two-terminal lateral Fe_3O_4/n-doped GaAs(100) thin layer/Fe_3O_4 spin-valve (SV) device. The bias-dependent room-temperature MR effect is observed, which demonstrates the all-electric spin injection and detection from a magnetic half-metal to a semiconductor at room temperatures.

2. Experiments

Firstly, an ultrathin Fe_3O_4 film was epitaxially grown on a GaAs(100) substrate. The GaAs(100) wafer used in this study consisted of epilayers of n-GaAs with the following structure: amorphous As-cap/n-GaAs (500 nm, 3×10^{18} cm^{-3})/500 μm thick semi-insulating (S.I.) GaAs(100). After cleaned in acetone and IPA thoroughly, GaAs wafer was loaded into a UHV-MBE chamber with a base pressure of 2×10^{-10} mbar and annealed at 830 K for 30 min to desorb the capped As layer

†Corresponding author. E-mail: yazhai@seu.edu.cn
‡Corresponding author. E-mail: ybxu@nju.edu.cn

© 2022 Chinese Physical Society and IOP Publishing Ltd

and form a smooth single crystalline GaAs surface. By using the postgrowth oxidation method,[30] a thickness of 4 nm Fe film was deposited on top of the GaAs wafer at a chamber pressure better than 1×10^{-9} mbar at room temperature, using e-beam evaporator at a rate of 2 Å/min, followed by oxidizing in an oxygen environment of 5×10^{-5} mbar for 10 min at 500 K. The growth process of the single crystalline magnetite film was monitored by reflection high-energy electron diffraction (RHEED). The RHEED patterns of Fe_3O_4 film along the GaAs[0$\bar{1}$1] axis is shown in Fig. 1(a), which suggests the epitaxial growth.

A local geometry with four contacts is used to measure the spin signal of the lateral spin valve structure, as schematically shown in Fig. 1(b). Subsequently, two Fe_3O_4 electrodes ($Fe_3O_4$1: 17×156 μm, $Fe_3O_4$2: 97×156 μm) with an edge to edge distance of 2.6 μm were patterned by the electron beam lithography, optical lithography and selective H_2SO_4-based etchant. The scanning electron microscope image of two Fe_3O_4 electrodes is shown in Fig. 1(c). Finally, four Au electrodes were fabricated by optical lithography and lift-off process. The total fabrication process of the Fe_3O_4/n-GaAs/Fe_3O_4 spin valve device is summarized in Fig. 1(d). Subsequently, all terminals are wire bonded to a chip and connected to Keithley Source Meter 2450 for magnetic transport measurements.

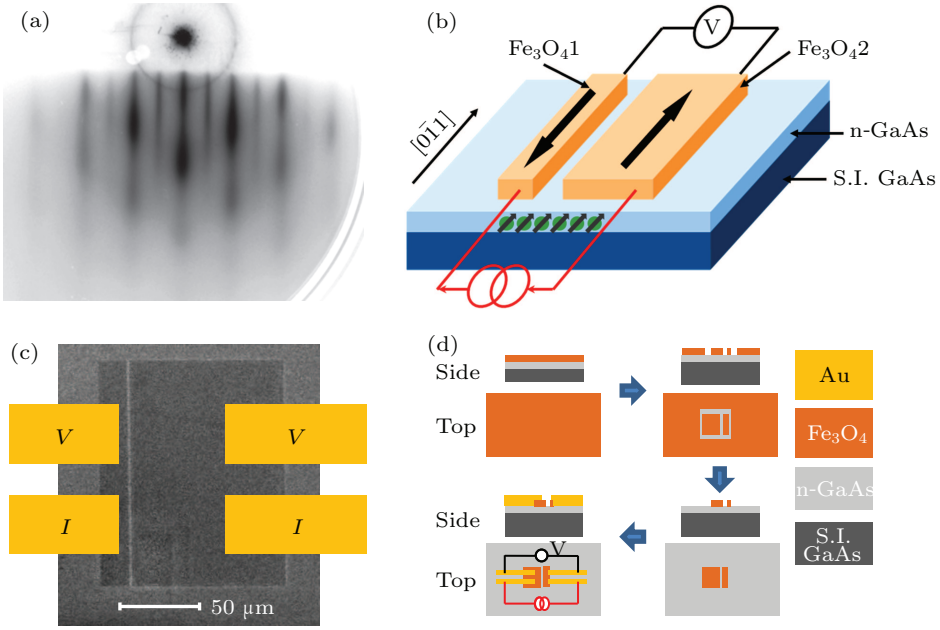


Fig. 1. (a) RHEED patterns of Fe_3O_4 with the electron beam along GaAs(100)[0$\bar{1}$1] direction. (b) Schematic diagram of the two-terminal lateral device. (c) Typical SEM image of the fabricated Fe_3O_4/GaAs/Fe_3O_4 device. (d) Illustration of the fabrication process of the device.

3. Results and discussion

The in-plane magnetic anisotropy of Fe_3O_4/GaAs film obtained by ferromagnetic resonance is shown in Fig. 2(a). It is seen that the film shows a dominant uniaxial symmetry with its easy axis (EA) along [0$\bar{1}$1] ($\varphi_H = 0°$). An additional small four-fold symmetry is observed clearly with its EA along [010] and [001]($\varphi_H = 45°$ and 135°, respectively), which reveals a dominant uniaxial magnetic anisotropy (UMA) plus a minor cubic magnetic anisotropy in our ultrathin Fe_3O_4 single crystal film. The UMA is induced by the GaAs substrate due to the interfacial effect between Fe_3O_4 and GaAs, which may originate from the unidirectional chemical bonding and the anisotropic lattice relaxation, while the four-fold magnetic anisotropy originates from the cubic magnetocrystalline anisotropy of bulk Fe_3O_4.[31] By fitting the experimental angular dependence of the resonance field data with saturation magnetization $M_s = 470$ Gs obtained by vibrating sample magnetometry (VSM), the UMA constant is determined as 5.7×10^4 erg/cm^3 and the magnetocrystalline anisotropy constant is determined as -3.1×10^4 erg/cm^3, about 26% of the value of bulk Fe_3O_4 (-11.8×10^4 erg/cm^3)[32] due to the interfacial effect and the lattice relaxation at the Fe_3O_4/GaAs interface. The Kerr loop with the applied field along the EA of UMA (GaAs(100)[0$\bar{1}$1]) direction is measured, as shown in Fig. 2(b). It shows a perfect square loop with the squareness of 96% and the coercivity of 130 Oe, which suggests that the EA of UMA direction is perfect for the magnetic electrode of the spin injection and detection device.

For fabricating the epitaxial Fe_3O_4/GaAs two-terminal devices, the long edges of the two Fe_3O_4 electrodes are along EA of Fe_3O_4. The local spin valve (LSV) structure with a four-terminal setup was used to measure the spin transport effects of the device and the external magnetic field was applied in-plane to magnetize the Fe_3O_4 electrodes (see Fig. 1(c)). We intentionally induced shape anisotropy between the two Fe_3O_4 electrodes, where the aspect ratios of two Fe_3O_4 electrodes as

1:9 and 6:9 were chosen respectively. Combining with the strong interfacial UMA, a large difference in coercivity can be expected. To ascertain this, we measured the magnetic hysteresis loops of $Fe_3O_4$1 and $Fe_3O_4$2 at room temperature by focused magneto-optical Kerr effect (FMOKE) with a spot size less than 1 μm, which consists of a stabilized 5 mW continuous HeNe laser of 635 nm wavelength, a stack of focusing lenses and a nano-positioning stage, as shown in Fig. 3. From the magnetic hysteresis loops, we can see both high squareness and sharp magnetization switching, and 37 Oe and 28 Oe of coercivity corresponding to $Fe_3O_4$1 and $Fe_3O_4$2 electrodes, respectively, can be distinguished, which are very important for further MR measurements.

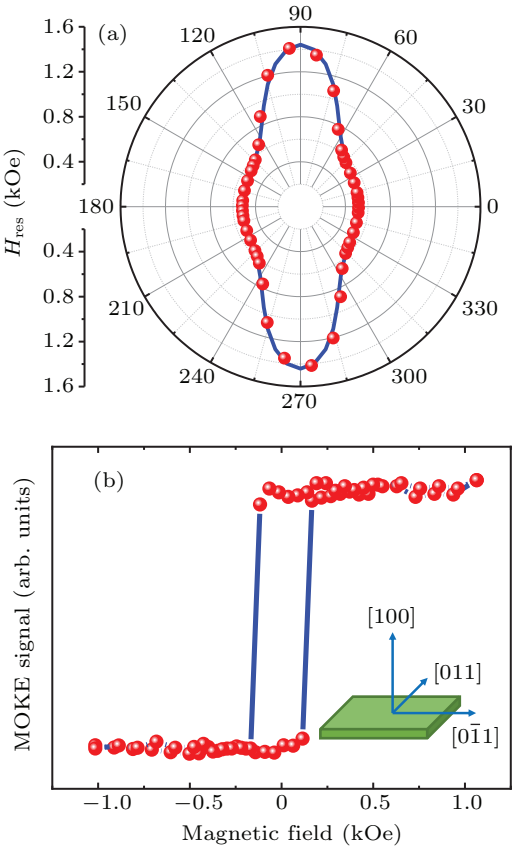


Fig. 2. (a) The ferromagnetic resonance field as a function of the in-plane field orientation with 0° along GaAs(100)[0$\bar{1}$1] direction. The circles are the experimental data points and the solid lines represent the theoretical fitted curves. (b) The Kerr loop with the applied field along GaAs(100)[0$\bar{1}$1] direction.

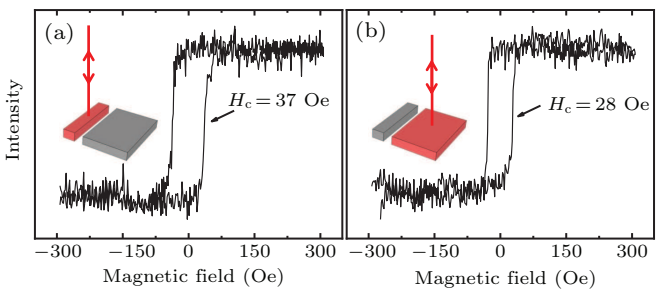


Fig. 3. Magnetic hysteresis loops of the Fe_3O_4 electrode (a) 1 and (b) 2, respectively, characterized by magneto-optical Kerr effect (MOKE) at room temperature. The insets are indicated the position of laser spot.

Figure 4(a) displays nonlinear and symmetric current–voltage (I–V) characteristics for the device. Here, the nonlinearity agrees with the expected non-Ohmic contacts between the n-GaAs layer and the Fe_3O_4 electrodes, and the symmetrical I–V curve reveals that the barrier height between two Fe_3O_4 electrodes and GaAs is nearly the same.[33] The working principle of the two-terminal SV device is elucidated using a simple electrical circuit, as shown in the inset of Fig. 4(a). To take into account the Fe_3O_4/n-GaAs Schottky barriers in the actual device,[27] this circuit consists of two diodes D, each contributing a parallel resistance of R_D due to potential diode imperfections. Since the two energy barriers are always oppositely biased, the diodes are assigned to connect back-to-back in series with an additional resistance R_{GaAs}, given by the GaAs layer. By using the thermionic-field emission model,[34] the device current I, which associates with the Schottky barrier height φ and the tunnelling parameter, can be defined as $I = I_S(e^{qV/\beta kT} - 1)$, where $I_S = SAT^2 e^{-q\varphi/kT}$, and β and I_S can be obtained from the logarithmic plot in Fig. 4(b). Therefore, the barrier heights of the $Fe_3O_4$1 and $Fe_3O_4$2 contacts have also been determined as 0.36 ± 0.02 eV, which agrees with our previous electrical characterization of Fe_3O_4/n-GaAs films.[26]

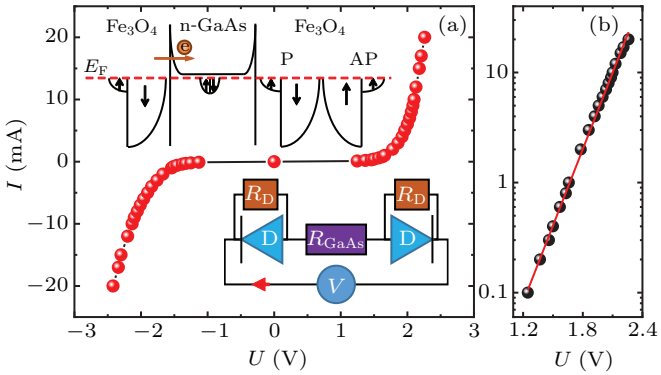


Fig. 4. (a) Four-point I–V characteristics of the device at room temperature. Inset shows the band structure (upper row) and a back-to-back diode circuit configuration for the electrical measurement (lower row). D refers to the Fe_3O_4/GaAs Schottky contact. The parallel resistors R_D represent conduction paths due to potential diode imperfections at the Fe_3O_4/GaAs interfaces. (b) Logarithmic plot of the I–V curve. The linear dependence of the current is numerically fitted.

The device MR is performed with different applied currents at room temperature, and the magnetic field sweeps from −250 Oe to 250 Oe. The resistance of the spin valve device is around 390 Ω, and the signal-to-noise ratio is better than 5×10^{-6}. With lineally fitting of the background of the raw data, the MR data with this background subtracted with different applied currents of 5 mA, 8 mA and 10 mA are shown in Fig. 5(a). Here the MR is defined as MR $= (R_{AP} - R_P)/R_P$, with R_P and R_{AP} being the device resistances at the parallel and antiparallel states, respectively. As the magnetic field sweeps, an obvious MR effect can be distinguished, which is

largely different from our previous anisotropic magnetoresistance (AMR) on Fe_3O_4/GaAs film.[26] With a high magnetic field, $Fe_3O_4$1 and $Fe_3O_4$2 are in a spin parallel state, leading to a small resistance. The resistance reaches the maximum value near the applied field of 32 ± 3 Oe, which is the average of coercivity of $Fe_3O_4$1 and $Fe_3O_4$2 electrodes, where $Fe_3O_4$1 and $Fe_3O_4$2 are in a spin antiparallel state.

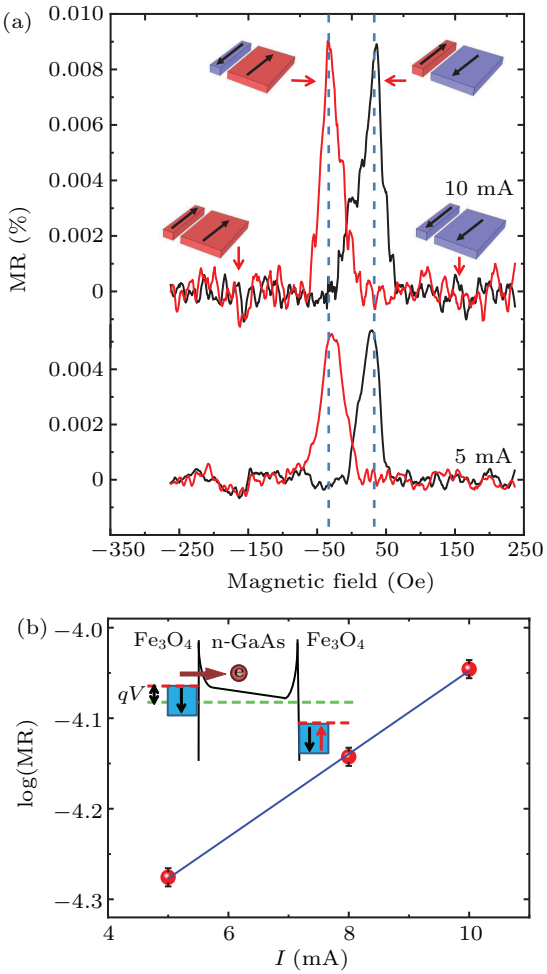


Fig. 5. (a) The bias-dependent MR effect of the device with current of 5 mA (upper row), and 10 mA (lower row). (b) The dependence of logarithm of MR ratio and the applied current. The inset shows the schematics of the device band diagrams under bias conditions. Here, qV refers to the band offsets under a bias.

Therefore, it can be inferred that the MR effect is originated from the two spin configurations of $Fe_3O_4$1 and $Fe_3O_4$2 electrodes, and the spin current is indeed injected from $Fe_3O_4$1/$Fe_3O_4$2 to n-GaAs layer and transferred through n-GaAs channel, and eventually detected by the other $Fe_3O_4$2/$Fe_3O_4$1 electrodes at room temperature. The switching of MR loop is slower than the MOKE result, which may originate from the tunnelling AMR. As increasing the applied current from 5 mA to 10 mA, the bias voltage increases and the MR ratio increases from 0.0053% to 0.0090%. The MR ratio accords logarithmic relationship with the applied current, as can be seen from Fig. 5(b), consistent with the tunnelling model, and the increase of bias voltage leads to the higher probability of tunnelling through the Schottky barrier. The inset of Fig. 5(b) shows the schematic band structure of the device under biased conditions. When the bias voltage increases, the MR ratio increases, which is associated with an increased number of electrons from the injector contact tunnelling into the GaAs layer. Here, it can be deduced that the observed bias-dependent MR confirms the electrical spin injection and detection in our two-terminal SV device.

4. Conclusion and perspectives

In summary, we have demonstrated a bias-dependent spin injection and detection related MR effect in the two-terminal Fe_3O_4/n-GaAs(100)/Fe_3O_4 lateral spin-valve device. The nonlinear and symmetric current–voltage (I–V) characteristic is observed for the device and the Schottky barrier height is calculated as 0.36 eV. The two Fe_3O_4 electrodes along the magnetic easy axis of the film are fabricated to have different switching fields, which leads to clear MR effect at room temperature due to the parallel and anti-parallel alignments. The MR effect shows a strong bias dependence under different applied current, further confirming the spin injection across the Fe_3O_4/GaAs interface. Our work has demonstrated the feasibility in developing the room temperature two terminals lateral spin valve device without tunnelling spacer, which has potential applications for the high density spin FET devices.

Acknowledgements

Project supported by the National Key Research and Development Program of China (Grant No. 2017YFA0204800), and the National Natural Science Foundation of China (Grant Nos. 52071079 and 11504047).

References

[1] Datta S and Das B 1990 *Appl. Phys. Lett.* **56** 665
[2] Zutic I, Fabian J and Das Sarma S 2004 *Rev. Mod. Phys.* **76** 323
[3] Wang L, Chen L C, Liu W Y, Han S, Wang W W, Lu Z J and Chen S S 2018 *Chin. Phys. B* **27** 097202
[4] Gu X R, Guo L D and Sun X N 2018 *Chin. Phys. B* **27** 107202
[5] Benítez L A, Sierra J F, Torres W S, Arrighi A, Bonell F, Costache M V and Valenzuela S O 2018 *Nat. Phys.* **14** 303
[6] Liu T, Wang X, Wang H, Shi G, Gao F, Feng H, Deng H, Hu L, Lochner E, Schlottmann P, von Molnár S, Li Y, Zhao J and Xiong P 2020 *ACS Nano* **14** 15983
[7] Kikkawa J M and Awschalom D D 1998 *Phys. Rev. Lett.* **80** 4313
[8] Kikkawa J M and Awschalom D D 1999 *Nature* **397** 139
[9] Lou X, Adelmann C, Crooker S A, Garlid E S, Zhang J, Reddy K S M, Flexner S D, Palmstrøm C J and Crowell P A 2007 *Nat. Phys.* **3** 197
[10] Van't Erve O M J, Li C H, Kioseoglou G, Hanbicki A T, Osofsky M, Cheng S F and Jonker B T 2007 *Appl. Phys. Lett.* **91** 122515
[11] Dash S P, Sharma S, Patel R S, de Jong M P and Jansen R 2009 *Nature* **462** 491
[12] Bhat S G and Kumar P S A 2014 *Sci. Rep.* **4** 6296
[13] Tombros N, Jozsa C, Popinciuc M, Jonkman H T and van Wees B J 2007 *Nature* **448** 571
[14] Dlubak B, Martin M B, Deranlot C, Servet B, Xavier S, Mattana R, Sprinkle M, Berger C, De Heer WA, Petroff F, Anane A, Seneor P and Fert A 2012 *Nat. Phys.* **8** 557
[15] Fert A and Jaffres H 2001 *Phys. Rev. B* **64** 184420

[16] Wong P K J, Zhang W, Wu J, Will I G, Xu Y B, Xia K, Holmes S N, Farrer I, Beere H E and Ritchie D A 2016 *Sci. Rep.* **6** 29845

[17] Dedkov Y S, Rudiger U and Guntherodt G 2002 *Phys. Rev. B* **65** 064417

[18] Lu X Y, Atkinson L J, Kuerbanjiang B, Liu B, Li G Q, Wang Y C, Wang J L, Ruan X Z, Wu J, Evans R F L, Lazarov V K, Chantrell R W and Xu Y B 2019 *Appl. Phys. Lett.* **114** 192406

[19] Rakshit R, Hattori A N, Naitoh Y, Shima H, Akinaga H and Tanaka H 2019 *Nano Lett.* **19** 5003

[20] Fonin M, Pentcheva R, Dedkov Yu S, Sperlich M, Vyalikh D V, Scheffler M, Rüdiger U and Güntherodt G 2005 *Phys. Rev. B* **72** 104436

[21] Schmidt G, Ferrand D, Molenkamp L W, Filip A T and van Wees B J 2000 *Phys. Rev. B* **62** R4790

[22] Fert A and Jaffres H 2001 *Phys. Rev. B* **64** 184420

[23] Jonker B T, Kioseoglou G, Hanbicki A T, Li C H and Thompson P E 2007 *Nat. Phys.* **3** 542

[24] Oltscher M, Ciorga M, Utz M, Schuh D, Bougeard D and Weiss D 2014 *Phys. Rev. Lett.* **113** 236602

[25] Kountouriotis K, Barreda J L, Keiper T D, Zhang M and Xiong P 2018 *Nano Lett.* **18** 4386

[26] Hassan S S A, Xu Y B, Ahmad E and Lu Y X 2007 *IEEE Trans. Magn.* **43** 2875

[27] Watts S M, Boothman C, van Dijken S and Coey J M D 2005 *Appl. Phys. Lett.* **86** 212108

[28] Koo H C, Kwon J H, Eom J, Chang J, Han S H and Johnson M 2009 *Science* **325** 1515

[29] Huang Z C, Liu W Q, Yue J J, Zhou Q H, Zhang W, Lu YX, Sui Y X, Zhai Y, Chen Q, Dong S, Wang J L, Xu Y B and Wang B P 2016 *ACS Appl. Mater. Interfaces* **8** 27353

[30] Lu Y X, Claydon J S, Xu Y B, Schofield D M, Thompson S M and van der Laan G 2004 *Phys. Rev. B* **70** 233304

[31] Zhai Y, Huang Z C, Fu Y, Ni C, Lu Y X, Xu Y B, Wu J and Zhai H R 2007 *J. Appl. Phys.* **101** 09D126

[32] Feng D, Ding S and Zhai H 1998 *Superconductivity and Magnetism* (Beijing: Science Press) p. 463 (in Chinese)

[33] Hirohata A, Xu Y B, Guertler C M, Bland J A C and Holmes S N 2001 *Phys. Rev. B* **63** 104425

[34] Sze S M and Ng K K 2006 *Physics of Semiconductor Devices* (New Jersey: John Wiley and Sons) p. 162